PHOTONICS Research

Influence of light pattern thickness on the manipulation of dielectric microparticles by optoelectronic tweezers

Shuailong Zhang,[1,2,3,4,5,9] Mohamed Elsayed,[4,5] Ran Peng,[6] Yujie Chen,[7] Yanfeng Zhang,[7] Steven L. Neale,[8] and Aaron R. Wheeler[3,4,5,10]

[1]School of Mechatronical Engineering, Beijing Institute of Technology, Beijing 100081, China
[2]Beijing Advanced Innovation Center for Intelligent Robots and Systems, Beijing Institute of Technology, Beijing 100081, China
[3]Department of Chemistry, University of Toronto, Toronto, Ontario M5S 3H6, Canada
[4]Institute of Biomedical Engineering, University of Toronto, Toronto, Ontario M5S 3G9, Canada
[5]Donnelly Centre for Cellular and Biomolecular Research, University of Toronto, Toronto, Ontario M5S 3E1, Canada
[6]Department of Marine Engineering, Dalian Maritime University, Dalian 116026, China
[7]State Key Laboratory of Optoelectronic Materials and Technologies, School of Electronics and Information Technology, Sun Yat-sen University, Guangzhou 510275, China
[8]James Watt School of Engineering, University of Glasgow, Glasgow G12 8QQ, UK
[9]e-mail: shuailong.zhang@bit.edu.cn
[10]e-mail: aaron.wheeler@utoronto.ca

Received 14 July 2021; revised 8 November 2021; accepted 23 November 2021; posted 24 November 2021 (Doc. ID 437528); published 27 January 2022

Optoelectronic tweezer (OET) is a useful optical micromanipulation technology that has been demonstrated for various applications in electrical engineering and most notably cell selection for biomedical engineering. In this work, we studied the use of light patterns with different shapes and thicknesses to manipulate dielectric microparticles with OET. It was demonstrated that the maximum velocities of the microparticles increase to a peak and then gradually decrease as the light pattern's thickness increases. Numerical simulations were run to clarify the underlying physical mechanisms, and it was found that the observed phenomenon is due to the co-influence of horizontal and vertical dielectrophoresis forces related to the light pattern's thickness. Further experiments were run on light patterns with different shapes and objects with different sizes and structures. The experimental results indicate that the physical mechanism elucidated in this research is an important one that applies to different light pattern shapes and different objects, which is useful for enabling users to optimize OET settings for future micromanipulation applications. © 2022 Chinese Laser Press

https://doi.org/10.1364/PRJ.437528

1. INTRODUCTION

Optoelectronic tweezer (OET) is an optical micromanipulation technology that relies on optically induced-dielectrophoresis (ODEP) force for the control of micro-/nano-scale objects [1–5]. Based on light patterned electric fields, OET is capable of exerting pico-to-nano Newton manipulation forces [6,7], and is well suited for parallel and independent control of multiple objects [1,3,8,9]. Because of these outstanding micromanipulation capabilities, OET has been widely used to manipulate and assemble bio-analytes and molecules [10–12], cells of different species [13–20], nano-/microparticles [8,21–26], electronic/photonic components [27–33], and microrobots [9], thus offering a powerful scientific tool to investigate the microscopic world for physical, chemical, and biological studies. More recently, OET technology has been successfully commercialized and used in the biopharmaceutical industry for antibody discovery and cell therapy development [34], demonstrating the prospect of this technology in both research and industrial settings.

In an OET system, the light pattern is a key factor that influences the moving behavior of the controlled micro-objects. Previous studies have shown that both the wavelength and optical intensity of light patterns can influence the performance of OET for particle manipulation [35,36]. However, for a given OET system with a fixed light source, there is little room to adjust the properties of the light to optimize the performance of the ODEP forces that enable OET applications. Therefore, in this work, we explored a more readily modifiable variable—the thickness of the projected light pattern—to study the effects of this variable on the movement of microparticles. Simulations in COMSOL Multiphysics (COMSOL Inc., USA) were

carried out to clarify the experimental results and provide insights to the physical mechanisms. It was demonstrated that thicker light patterns can induce stronger electric field gradients in the horizontal plane, exerting stronger horizontal DEP forces and thus a higher moving velocity for the microparticles. However, light patterns beyond a certain thickness can increase the DEP force in the vertical plane, making the microparticles escape from the OET trap at a lower horizontal moving velocity. Therefore, these two physical mechanisms should be considered when choosing the right parameters for light patterns to achieve optimal OET performance for micromanipulation. We show that this observation generally holds true for microparticles that experience negative DEP, but note that the relationship will be different for objects that experience positive DEP.

2. RESULTS AND DISCUSSION

Shown in Fig. 1(a) is a schematic of an OET device, comprising two plates. The top plate is an indium tin oxide (ITO)-coated glass slide; the bottom plate is also an ITO-coated glass slide, but with an additional photoconductive layer of hydrogenated-amorphous-silicon (a-Si:H) deposited onto it. The two plates were mounted together via a 150-μm-thick spacer to form a microchamber, in which the micromanipulation was performed. When a bias voltage is applied between the two plates and a light pattern is projected on the a-Si:H layer, a non-uniform electric field is generated in the liquid microchamber, which interacts with the micro-objects and produces DEP forces. If the micro-object is more polarizable than the surrounding medium [i.e., the real part of the Clausius–Mossotti (CM) factor is above zero], it will be attracted to the illuminated region due to a positive DEP force; if the micro-object is less polarizable than the surrounding medium (i.e., the real part of the CM factor is below zero), it will be repelled from the illuminated region due to a negative DEP force [37]. In this work, 10 μm diameter spherical polystyrene microbeads (Polysciences Inc., USA) were used, which were suspended in deionized water containing Tween 20 (0.05% volume fraction) and pipetted into the microchamber of the OET device. The OET device was driven by an AC potential ($10 V_{pp}$ 20 kHz square wave). On applying the AC voltage, the polystyrene beads were repelled by the illuminated region due to the negative DEP force, allowing the use of hollow light patterns consisting of illuminated and dark regions to move and rotate the beads, as shown in Fig. 1(b) and Visualization 1 (clip 1). When a static light pattern is projected [Fig. 1(c)], the microbeads are repelled from the illuminated region and accumulate at the dark region, forming a desired micropattern [Fig. 1(d)]. More details can be found in Visualization 1 (clip 2). These results demonstrate the versatility of OET technology for microparticle manipulation based on different light patterns and also highlight the importance of investigating the influence of different light pattern parameters on electric field distribution and the related behavior of microparticles in an OET system.

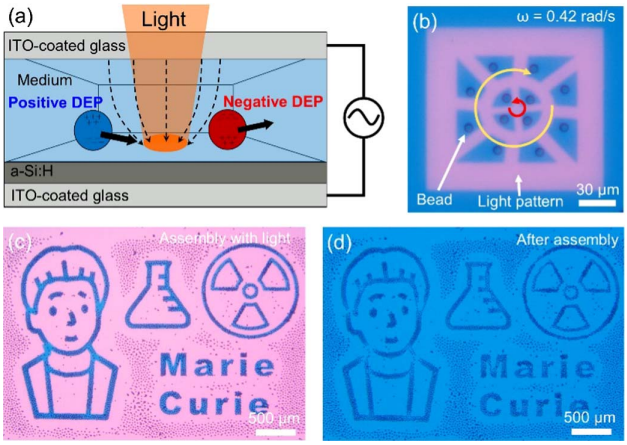

Fig. 1. (a) Schematic of an OET device, in which microparticles are manipulated via positive or negative DEP forces. (b) Video frame showing the use of dynamic light patterns to move/rotate multiple 10 μm polystyrene microbeads at an angular velocity of 0.42 rad/s. Red and yellow arrows represent the counterclockwise and clockwise rotational directions of the microbeads in the central and surrounding regions, respectively. Regions with red color represent the illuminated region, and regions with blue color represent the dark region. See Visualization 1 (clip 1) for more details. (c) Microscope image showing the illumination of the 10-μm-diameter microbead suspension with a light pattern depicting a stylized caricature of Marie Curie with symbols of an Erlenmeyer flask and radiation. Regions with red color represent the illuminated region, and regions with blue color represent the dark region. (d) Microscope image of the OET-assembled micropattern. See Visualization 1 (clip 2) for more details.

To investigate the influence of the light pattern on the ability to move microparticles, a single 10-μm-diameter bead was trapped by "doughnut"-shaped light patterns with a fixed inner diameter at 80 μm but different ring thicknesses, as shown in Figs. 2(a)–2(c) and Visualization 2 (noting that the doughnut shape is the most widely used light pattern shape for OET manipulation). In this case, the light pattern was kept stationary while the motorized stage was programmed to move linearly, which propelled the trapped bead to move in the opposite direction. Due to the viscous damped nature of the experiment, the beads quickly equilibrate to a constant velocity at which the DEP actuation force exerted on the bead is equal to the viscous drag force given by Stokes law [7,17,25,38], i.e.,

$$F_{\mathrm{DEP}} = F_{\mathrm{drag}} = 6\pi\eta r\nu, \tag{1}$$

where η is the viscosity of the liquid, r is the radius of the bead, and ν is the velocity of the bead. Since gravity forces the bead to sit in proximity to the a-Si:H surface, Faxen's correction was applied to adjust the calculation of the viscous drag force and the DEP force [6,17,38].

For each doughnut ring thickness evaluated, the maximum moving velocity of the bead was measured by gradually increasing the speed of the motorized stage, observing the velocity at which the bead fell out of the trap (see Visualization 2, clip 4). As shown in Fig. 2(d), the maximum moving velocity of the bead increases rapidly to a peak and then slightly decreases as the ring thickness increases from 2.5 to 135 μm. Using Eq. (1), these data correlate with DEP forces, which range from around 20 pN to more than 100 pN for the condition with highest force and velocity, found with a ring thickness of 20 μm. These experimental results demonstrate the influence of light pattern thickness on the maximum velocity of a microparticle under OET manipulation. The sharp increase in force

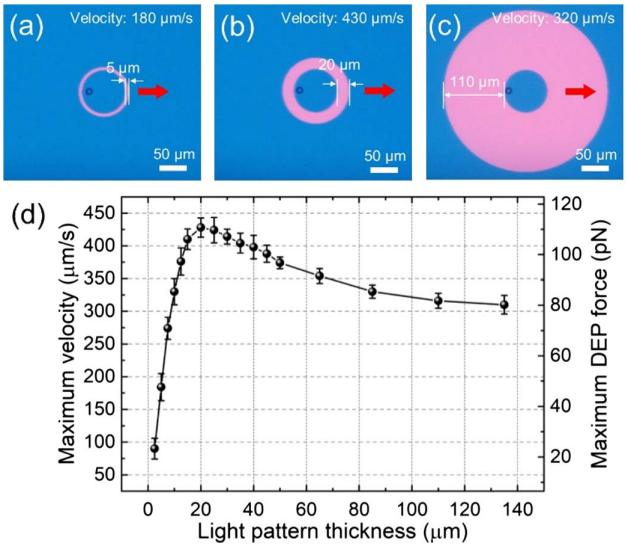

Fig. 2. (a)–(c) Microscope images of a 10 μm polystyrene microbead trapped by doughnut-shaped light patterns with the same inner diameter but different ring thicknesses (i.e., 5 μm, 20 μm, and 110 μm), and moving at 180 μm/s, 430 μm/s, and 320 μm/s, respectively. See Visualization 2 (clips 1–3) for more details. The red arrow represents the moving direction. (d) Maximum velocity (left axis) and maximum DEP force (right axis) versus light pattern's ring thickness. The velocity refers to the velocity of microbeads in the horizontal direction. Error bars represent the standard deviation for five replicates.

available as the ring thickness increased from 2.5 to 20 μm was expected; however, the decrease in force exerted on particles at greater thickness was counterintuitive and prompted further investigation. For light patterns increased to above 135 μm (e.g., 200 μm thickness), the maximum velocity of the microbead saturates at around 300 μm/s.

To probe the phenomenon of reduced force found for thick doughnut rings and to clarify the physical mechanism for the observed experimental results, simulations were carried out in COMSOL Multiphysics using the AC/DC module (COMSOL Inc., Burlington, MA, accessed via license obtained through CMC Microsystems, Kingston, Canada) [6–9]. The model length (x axis) and height (y axis) were set to 500 μm and 150 μm, respectively. The OET trap created by the doughnut-shaped light pattern is located at the bottom of the model, with its inner diameter set to 80 μm and thickness set to different values used in the experiment (using the parameter sweep function). The conductivities of the illuminated and dark regions were set to 10^{-4} S/m and 10^{-6} S/m, respectively. Other simulation parameters (voltage, frequency, etc.) were set according to the experimental parameters (square wave, 10 V, 20 kHz). To simulate the electric potential distribution, the AC/DC module of COMSOL Multiphysics was applied, and specific boundary conditions were implemented for the model. In this work, electric insulation was set for the sides of the model, and the top side of the model was set as ground (0 V), while the bottom side of the model was given an electric potential of 10 V. Different parts in the simulation model were defined as sub-domains, and the interfaces between different sub-domains were set to a continuity boundary condition. Then, the electric potential and electric field were computed by solving the continuity equations

$$\nabla \cdot J = Q_{j,v}, \tag{2}$$

$$J = \sigma E + j\omega D + J_e, \tag{3}$$

$$E = -\nabla V, \tag{4}$$

where J is the current density, $Q_{j,v}$ is the volumetric source of current, σ is the electrical conductivity, E is the electric field, ω is the angular frequency, D is the electric displacement, J_e is the externally generated current density, and V is the applied electrical potential.

Shown in Figs. 3(a) and 3(b) are the heat maps of the simulated electric potential and electric field distribution (i.e., cross-sectional view of an OET device). As shown, there is a big potential change at the edge of the light pattern resulting in a region of strong electric field with sharp field variation. This is caused by the difference in conductivity between the illuminated and dark a-Si:H surfaces. Since the bead reaches its maximum velocity at the edge of the light pattern, it is here that we investigate the DEP manipulation force exerted on the bead. Based on classic DEP theory for spherical microparticles [37], the DEP force is given by

$$F_{\mathrm{DEP}} = 2\pi r^3 \varepsilon_m \mathrm{Re}[K(\omega)] \nabla E^2, \tag{5}$$

where r is the radius of the bead, ε_m is the permittivity of the medium, $\mathrm{Re}[K(\omega)]$ is the real component of the CM factor, and ∇E^2 is the gradient of the external electric field's square. Therefore, the DEP force exerted on the microbead is proportional to the gradient of the electric field square (i.e., $F_{\mathrm{DEP}} \propto \nabla E^2$). This equation has been shown to provide a decent approximation of the DEP forces in OET devices [35,37,39]. Based on the electric field distribution in Fig. 3(b), the gradients of electric field squared in x and y directions (i.e., in horizontal and vertical planes) at the edge of the light pattern can be calculated for light patterns with different thicknesses, as shown in Fig. 3(c) and 3(d), respectively. Based on the results in Fig. 3(c), it can be inferred that the horizontal DEP force exerted to the bead increases as the light pattern thickness increases, and the force saturates after the light pattern thickness reaches 20 μm. In addition, based on the results in Fig. 3(d), it can be inferred that the vertical DEP force exerted on the bead increases as the light pattern thickness increases, and no sign of force saturation is observed. These simulation results provide important insights into the physical mechanism for the observed phenomenon related to the movement of microbeads when they are manipulated by doughnut-shaped rings with different thicknesses. When the ring thickness increases up to around 20 μm, the horizontal DEP force also increases (relative to the drag force), causing the maximum velocity of the bead to increase. This effect saturated for ring thicknesses of around 20 μm, and for ring thicknesses greater than this value, the vertical DEP force increases, which imparts increasing z-axis DEP forces (pointing into solution), which can lift the bead and make it escape with a hop out of the trap. This interesting z-axis bead escape mechanism (i.e., hopping behavior) was investigated in our previous work and was

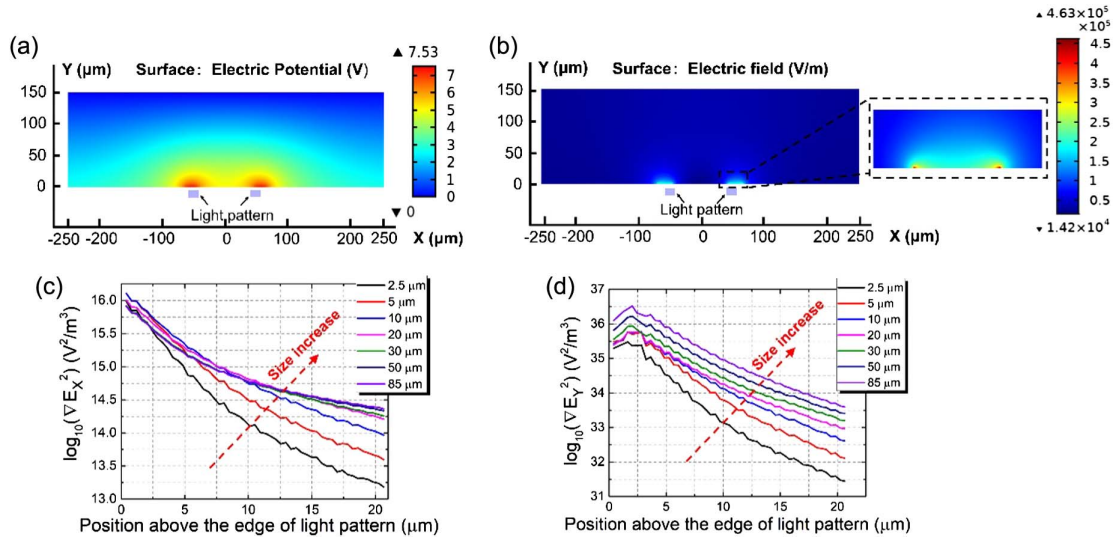

Fig. 3. Plots of (a) simulated electric potential, and (b) simulated electric field for an OET trap formed by illuminating a doughnut-shaped light pattern on the photoconductive layer of an OET device. The simulated electric potential and electric field are plotted in heat maps (blue, low; red, high). The inset in (b) is a magnified view of the main-panel data in the dashed square. Simulated gradients of electric field square (c) along x axis (horizontal plane) and (d) y axis (vertical plane) above the edge of light patterns with different thicknesses (2.5–85 μm).

shown to be mainly due to a vertical DEP force [40]. Therefore, for light patterns above 20 μm, the induced horizontal DEP forces are similar, but the induced vertical DEP forces are stronger for light patterns with larger thicknesses. As a result, the bead is more likely to be lifted up when manipulated by light patterns with larger thicknesses and thus can escape the OET trap at a slightly lower velocity. This explains why the moving velocity of the bead increases to a peak and then starts to decrease as the light pattern thickness increases (Fig. 2).

To test the universality of the physical mechanism, rectangular-shaped light patterns with fixed length at 270 μm but different thicknesses were used to manipulate a microbead, as shown in Figs. 4(a)–4(c) and Visualization 3 (noting that rectangular-shaped light patterns are widely used for cell/microparticle sorting in OET-integrated microfluidic devices [17,41–46]). The maximum velocity and maximum DEP force of the bead were measured/calculated accordingly, as shown in Fig. 4(d). For a given microbead manipulated by rectangular-shaped light patterns with different thicknesses, its maximum velocity and maximum DEP force increase rapidly to a peak and then slightly decrease as the light pattern thickness increases from 2.5 to 135 μm. These results are similar to those observed experimentally for doughnut-shaped light patterns, suggesting the underlying physical mechanism is an important one that applies for light patterns with different shapes, although the optimal thickness will change slightly for differently shaped light patterns. It is also observed that the maximum velocities are smaller for rectangular light patterns than their doughnut-shaped counterparts for similar thickness, which is mainly due to the curved boundary of doughnut-shaped light patterns and a larger interactive interface/region with the microparticle.

Finally, motivated by the recent report of OET-driven micromachines formed from circular micro-gear structures [47], we applied similar techniques to evaluate effects on micro-gears, depicted in Fig. 5(a). The micro-gears used here are formed from SU8 (Kayaku Advanced Materials) and are fabricated using standard photolithography techniques [9]. They have a diameter of 200 μm and a height of 60 μm, much larger than the 10-μm-diameter polystyrene microbeads described above.

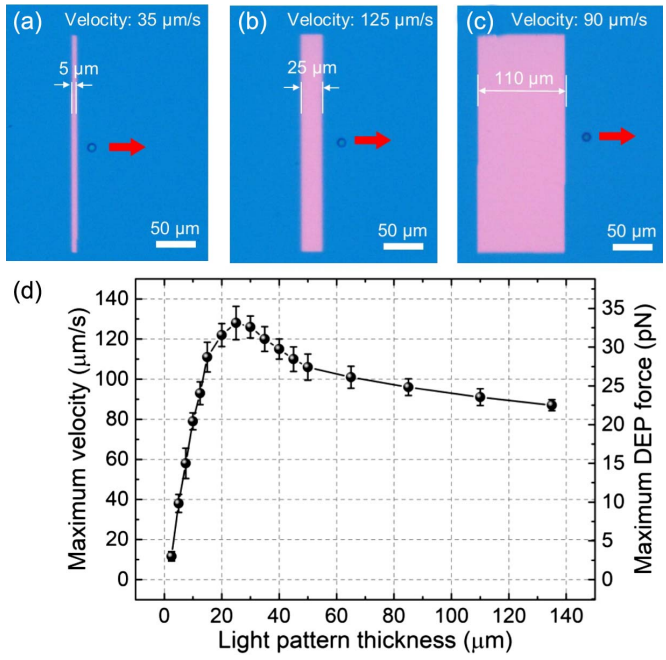

Fig. 4. (a)–(c) Microscope images of a 10 μm polystyrene microbead moved by rectangular-shaped light patterns with the same length but different thicknesses (i.e., 5 μm, 25 μm, and 110 μm), and moving at 35 μm/s, 125 μm/s, and 90 μm/s, respectively. The red arrow represents the moving direction. See Visualization 3 for more details. (d) Maximum velocity (left axis) and maximum DEP force (right axis) versus light pattern's thickness, in which error bars represent the standard deviation for five replicates. The velocity refers to the velocity of microbeads in the horizontal direction.

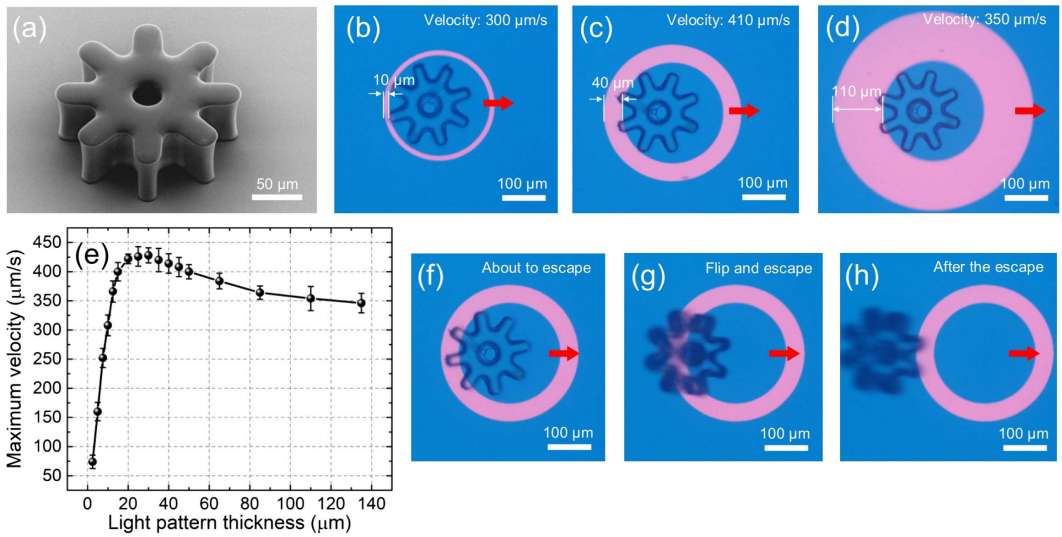

Fig. 5. (a) SEM image of a micro-gear. (b)–(d) Microscope images of a micro-gear trapped by doughnut-shaped light patterns with the same inner diameter but different ring thicknesses (i.e., 10 μm, 40 μm, and 110 μm), and moving at 300 μm/s, 410 μm/s, and 350 μm/s, respectively. The red arrow represents the moving direction. See Visualization 4 (clips 1–3) for more details. (e) Maximum velocity of the micro-gear versus light pattern's thickness, and the error bars represent the standard deviation for five replicates. The velocity refers to the velocity of micro-gears in the horizontal direction. (f)–(h) Microscope images showing the escape of a micro-gear from an OET trap with flipping behavior. See Visualization 4 (clip 4) for more details.

Regardless, micro-gears can be made to move at different velocities using doughnut-shaped light patterns with different ring thicknesses, as shown in Figs. 5(b)–5(d) and Visualization 4 (clip 1–3). The maximum velocities of the micro-gears were measured for light patterns with different ring thicknesses, as shown in Fig. 5(e). A similar trend was observed as for cases with microbeads, in which the maximum velocity increases to a peak at around 425 μm/s and then slightly decreases as the light pattern thickness increases. These results demonstrate the importance of the physical mechanisms governing the behavior of micro-objects regardless of the size, structure, and material of micro-objects when they are manipulated by OET with light patterns of different thicknesses.

The asymmetry of the particles in micro-gear experiments (relative to the symmetric spherical beads described above) provides additional substantiation of the "vertical DEP" hypothesis. Shown in Figs. 5(f)–5(h) are microscope images of a micro-gear escaping from a doughnut-shaped light pattern (from Visualization 4, clip 4). Presumably caused by the vertical DEP force, the micro-gear is lifted up and seems to "flip" in the medium as it escapes the OET trap. These results help visualize the process through which micro-objects escape a trap in an OET system upon reaching its maximum moving velocity and also highlight the influence of the vertical DEP force and related lifting effect on micro-objects under OET manipulation. Similar phenomena were also observed for polystyrene microbeads (see Visualization 2, clip 4).

For micro-objects that experience positive DEP, such as metallic microparticles [6], we did not observe the phenomenon reported in this work. The main reason is that microparticles experiencing positive DEP forces will also experience positive vertical DEP forces, which pull down the microparticles toward the surface of the OET bottom plate instead of lifting them up.

In addition, we find in the experiments that different inner diameters of doughnut-shaped light patterns can significantly influence the maximum velocity of the particle experiencing negative DEP. However, this is likely due to a different mechanism. For light patterns with fixed pattern thicknesses but different inner diameters, the interactive interface/region between the light boundary and the microparticle is different (due to different curvature of the boundary). For example, if the inner diameter of the light pattern is small enough (with a size similar to the particle), the doughnut-shaped light pattern will function like a solid circular light pattern and start to repel the particle, making it escape from the central dark region, and the moving velocity is not measurable. These results demonstrate the important and complex nature of light pattern layout on the behaviors of micro-objects under OET manipulation, which normally involves several physical mechanisms for different circumstances and is worthy of continuing study in the future.

3. CONCLUSION

In conclusion, we studied the influence of light pattern thickness on the ability to move microparticles and micro-gears manipulated by OET. The experiments were supported by numerical simulations. It was found that the light pattern thickness can influence both horizontal and vertical DEP forces, leading to first an increase and then a decrease of the maximum velocity achievable by the micro-object as the light pattern thickness increases. This result provides important insight about the optimization of light pattern parameters to achieve better OET performance for micromanipulation applications. In particular, users who employ negative DEP in their experiments should consider both horizontal and vertical DEP forces when selecting the appropriate light pattern parameters to

increase the moving velocities of micro-objects and exert stronger manipulation forces, which is important for improving OET performance for many micromanipulation applications.

4. METHODS

The OET setup comprises a digital mirror device (DMD) pattern illuminator (Mightex Polygon 1000, 625 nm, 1100 mW LED source) interfaced with an upright optical microscope (Nikon Eclipse Ni-E microscope integrated with Märzhäuser Scan Plus 130-85 motorized stage and LW scientific MiniVID CMOS camera). The average power density of projected light patterns remains constant at 0.44 W/cm^2 as measured using a Thorlabs PM16-130 power meter. A user-friendly software (Nikon NIS Elements Software platform) was used to control the microscope, camera, and motorized stage. OET devices were similar to those reported previously [25,40], consisting of a 20 μL fluidic chamber sandwiched between two glass plates separated by a 150 μm spacer. The plates were coated with a thin layer of ITO, and the bottom plate was coated with an additional layer of 1-μm-thick a-Si:H, applied via radio frequency plasma-enhanced chemical vapor deposition. The AC potential ($10 V_{pp}$, 20 kHz, square wave) used to drive the OET device was supplied by a function generator (Agilent 33220A) and an amplifier (Thurlby Thandor Instrument WA31). At this bias condition, the real part of the CM factor is negative for particles (polystyrene beads and polymer micro-gears) and liquid media (aqueous solutions with conductivity < 10 mS/m) used here.

Suspensions of polystyrene microparticles (10 μm diameter, Polysciences) were formed at 10^6 to 10^7 particles per milliliter in liquid medium (deionized water containing 0.05% volume ratio of Tween 20, P9416 Sigma) prior to loading into the OET devices. Micro-gears were formed from SU-8 2050 (Kayaku Advanced Materials) at the University of Toronto's Centre for Research and Applications in Fluidic Technologies (CRAFT) cleanroom facility using methods similar to those reported previously [9]. The SEM image for the micro-gear was collected using an environmental SEM (QUANTA FEG 250 ESEM), with a pressure of 130 Pa and an electron beam with 10 keV energy and 3 nm spot size.

Funding. National Natural Science Foundation of China (11774437, 61975243, 62103050); Natural Sciences and Engineering Research Council of Canada (ALLRP 548593-19, CREATE 482073-16, RGPIN 2019-04867, RTI-2019-00300).

Acknowledgment. The authors acknowledge the support from the Centre for Nanostructure Imaging at the Department of Chemistry, University of Toronto, for assistance in collecting SEM images, and the Centre for Research and Applications in Fluidic Technologies (CRAFT) for assistance in micro-gear fabrication. A. R. W. acknowledges the Canada Research Chair (CRC) program.

Disclosures. The authors declare no conflicts of interest.

Data Availability. Data underlying the results presented in this paper may be obtained from the authors upon reasonable request.

REFERENCES

1. P. Y. Chiou, A. T. Ohta, and M. C. Wu, "Massively parallel manipulation of single cells and microparticles using optical images," Nature **436**, 370–372 (2005).
2. M. C. Wu, "Optoelectronic tweezers," Nat. Photonics **5**, 322–324 (2011).
3. M. Woerdemann, C. Alpmann, M. Esseling, and C. Denz, "Advanced optical trapping by complex beam shaping," Laser Photon. Rev. **7**, 839–854 (2013).
4. Y. Huang, Z. Liang, M. Alsoraya, J. Guo, and D. Fan, "Light-gated manipulation of micro/nanoparticles in electric fields," Adv. Intell. Syst. **2**, 1900127 (2020).
5. H. Hwang and J. K. Park, "Optoelectrofluidic platforms for chemistry and biology," Lab Chip **11**, 33–47 (2011).
6. S. Zhang, Y. Liu, J. Juvert, P. Tian, J. C. Navaro, J. M. Cooper, and S. L. Neale, "Use of optoelectronic tweezers in manufacturing accurate solder bead positioning," Appl. Phys. Lett. **109**, 221110 (2016).
7. S. Zhang, J. Juvert, J. M. Cooper, and S. L. Neale, "Manipulating and assembling metallic beads with optoelectronic tweezers," Sci. Rep. **6**, 32840 (2016).
8. S. Zhang, Y. Zhai, R. Peng, M. Shayegannia, A. G. Flood, J. Qu, X. Liu, N. P. Kherani, and A. R. Wheeler, "Assembly of topographical micropatterns with optoelectronic tweezers," Adv. Opt. Mater. **7**, 1900669 (2019).
9. S. Zhang, E. Y. Scott, J. Singh, Y. Chen, Y. Zhang, M. Elsayed, M. D. Chamberlain, N. Shakiba, K. Adams, S. Yu, C. M. Morshead, P. W. Zandstra, and A. R. Wheeler, "The optoelectronic microrobot: a versatile toolbox for micromanipulation," Proc. Natl. Acad. Sci. USA **116**, 14823–14828 (2019).
10. D. Han and J. K. Park, "Optoelectrofluidic enhanced immunoreaction based on optically-induced dynamic AC electroosmosis," Lab Chip **16**, 1189–1196 (2016).
11. D. Han and J. K. Park, "Microarray-integrated optoelectrofluidic immunoassay system," Biomicrofluidics **10**, 034106 (2016).
12. Y. H. Lin, C. M. Chang, and G. B. Lee, "Manipulation of single DNA molecules by using optically projected images," Opt. Express **17**, 15318–15329 (2009).
13. Y. Zhang, J. Zhao, H. Yu, P. Li, W. Liang, Z. Liu, G. B. Lee, L. Liu, W. J. Li, and Z. Wang, "Detection and isolation of free cancer cells from ascites and peritoneal lavages using optically induced electrokinetics (OEK)," Sci. Adv. **6**, eaba9628 (2020).
14. S. Zhang, N. Shakiba, Y. Chen, Y. Zhang, P. Tian, J. Singh, M. D. Chamberlain, M. Satkauskas, A. G. Flood, N. P. Kherani, S. Yu, P. W. Zandstra, and A. R. Wheeler, "Patterned optoelectronic tweezers: a new scheme for selecting, moving, and storing dielectric particles and cells," Small **14**, 1803342 (2018).
15. S. Xie, X. Wang, N. Jiao, S. Tung, and L. Liu, "Programmable micrometer-sized motor array based on live cells," Lab Chip **17**, 2046–2053 (2017).
16. A. T. Ohta, M. Garcia, J. K. Valley, L. Banie, H. Y. Hsu, A. Jamshidi, S. L. Neale, T. Lue, and M. C. Wu, "Motile and non-motile sperm diagnostic manipulation using optoelectronic tweezers," Lab Chip **10**, 3213–3217 (2010).
17. S. B. Huang, M. H. Wu, Y. H. Lin, C. H. Hsieh, C. L. Yang, H. C. Lin, C. P. Tseng, and G. B. Lee, "High-purity and label-free isolation of circulating tumor cells (CTCs) in a microfluidic platform by using optically-induced-dielectrophoretic (ODEP) force," Lab Chip **13**, 1371–1383 (2013).
18. L. Y. Ke, Z. K. Kuo, Y. S. Chen, T. Y. Yeh, M. Dong, H. W. Tseng, and C. H. Liu, "Cancer immunotherapy μ-environment LabChip: taking advantage of optoelectronic tweezers," Lab Chip **18**, 106–114 (2018).
19. Y. Yang, Y. Mao, K. S. Shin, C. O. Chui, and P. Y. Chiou, "Self-locking optoelectronic tweezers for single-cell and microparticle manipulation across a large area in high conductivity media," Sci. Rep. **6**, 22630 (2016).
20. A. H. Jeorrett, S. L. Neale, D. Massoubre, E. Gu, R. K. Henderson, O. Millington, K. Mathieson, and M. D. Dawson, "Optoelectronic tweezers system for single cell manipulation and fluorescence imaging of live immune cells," Opt. Express **22**, 1372–1380 (2014).

21. A. Jamshidi, S. L. Neale, K. Yu, P. J. Pauzauskie, P. J. Schuck, J. K. Valley, H.-Y. Hsu, A. T. Ohta, and M. C. Wu, "Nanopen: dynamic, low-power, and light-actuated patterning of nanoparticles," Nano Lett. **9**, 2921–2925 (2009).
22. S. J. Lin, S. H. Hung, J. Y. Jeng, T. F. Guo, and G. B. Lee, "Manipulation of micro-particles by flexible polymer-based optically-induced dielectrophoretic devices," Opt. Express **20**, 583–592 (2012).
23. M. B. Lim, R. G. Felsted, X. Zhou, B. E. Smith, and P. J. Pauzauskie, "Patterning of graphene oxide with optoelectronic tweezers," Appl. Phys. Lett. **113**, 031106 (2018).
24. S. Liang, Y. Cao, Y. Dai, F. Wang, X. Bai, B. Song, C. Zhang, C. Gan, F. Arai, and L. Feng, "A versatile optoelectronic tweezer system for micro-objects manipulation: transportation, patterning, sorting, rotating and storage," Micromachines **12**, 271 (2021).
25. S. Zhang, W. Li, M. Elsayed, P. Tian, A. W. Clark, A. R. Wheeler, and S. L. Neale, "Size-scaling effects for microparticles and cells manipulated by optoelectronic tweezers," Opt. Lett. **44**, 4171–4174 (2019).
26. M. A. Zaman, P. Padhy, Y. T. Cheng, L. Galambos, and L. Hesselink, "Optoelectronic tweezers with a non-uniform background field," Appl. Phys. Lett. **117**, 171102 (2020).
27. A. Jamshidi, P. J. Pauzauskie, P. J. Schuck, A. T. Ohta, P. Y. Chiou, J. Chou, P. Yang, and M. C. Wu, "Dynamic manipulation and separation of individual semiconducting and metallic nanowires," Nat. Photonics **2**, 86–89 (2008).
28. Y. H. Lin, K. S. Ho, C. T. Yang, J. H. Wang, and C. S. Lai, "A highly flexible platform for nanowire sensor assembly using a combination of optically induced and conventional dielectrophoresis," Opt. Express **22**, 13811–13824 (2014).
29. H. Hwang, D. Han, Y. J. Oh, Y. K. Cho, K. H. Jeong, and J. K. Park, "In situ dynamic measurements of the enhanced SERS signal using an optoelectrofluidic SERS platform," Lab Chip **11**, 2518–2525 (2011).
30. M. B. Lim, J. L. Hanson, L. Vandsburger, P. B. Roder, X. Zhou, B. E. Smith, F. S. Ohuchi, and P. J. Pauzauskie, "Copper-and chloride-mediated synthesis and optoelectronic trapping of ultra-high aspect ratio palladium nanowires," J. Mater. Chem. A **6**, 5644–5651 (2018).
31. S. Zhang, Y. Liu, Y. Qian, W. Li, J. Juvert, P. Tian, J. C. Navarro, A. W. Clark, E. Gu, M. D. Dawson, J. M. Cooper, and S. L. Neale, "Manufacturing with light-micro-assembly of opto-electronic microstructures," Opt. Express **25**, 28838–28850 (2017).
32. M. C. Tien, A. T. Ohta, K. Yu, S. L. Neale, and M. C. Wu, "Heterogeneous integration of InGaAsP microdisk laser on a silicon platform using optofluidic assembly," Appl. Phys. A **95**, 967–972 (2009).
33. J. Juvert, S. Zhang, I. Eddie, C. J. Mitchell, G. T. Reed, J. S. Wilkinson, A. Kelly, and S. L. Neale, "Micromanipulation of InP lasers with optoelectronic tweezers for integration on a photonic platform," Opt. Express **24**, 18163–18175 (2016).
34. https://www.berkeleylights.com/.
35. W. Liang, S. Wang, Z. Dong, G. B. Lee, and W. J. Li, "Optical spectrum and electric field waveform dependent optically-induced dielectrophoretic (ODEP) micro-manipulation," Micromachines **3**, 492–508 (2012).
36. J. K. Valley, A. Jamshidi, A. T. Ohta, H. Y. Hsu, and M. C. Wu, "Operational regimes and physics present in optoelectronic tweezers," J. Microelectromech. Syst. **17**, 342–350 (2008).
37. R. Pethig, "Dielectrophoresis: status of the theory, technology, and applications," Biomicrofluidics **4**, 022811 (2010).
38. S. L. Neale, M. Mazilu, J. I. B. Wilson, K. Dholakia, and T. F. Krauss, "The resolution of optical traps created by light induced dielectrophoresis (LIDEP)," Opt. Express **15**, 12619–12626 (2007).
39. N. Liu, Y. Lin, Y. Peng, L. Xin, T. Yue, Y. Liu, C. Ru, S. Xie, L. Dong, H. Pu, H. Chen, W. J. Li, and Y. Sun, "Automated parallel electrical characterization of cells using optically-induced dielectrophoresis," IEEE Trans. Autom. Sci. Eng. **17**, 1084–1092 (2020).
40. S. Zhang, A. Nikitina, Y. Chen, Y. Zhang, L. Liu, A. G. Flood, J. Juvert, M. D. Chamberlain, N. P. Kherani, S. L. Neale, and A. R. Wheeler, "Escape from an optoelectronic tweezer trap: experimental results and simulations," Opt. Express **26**, 5300–5309 (2018).
41. W. Liang, L. Liu, H. Zhang, Y. Wang, and W. J. Li, "Optoelectrokinetics-based microfluidic platform for bioapplications: a review of recent advances," Biomicrofluidics **13**, 051502 (2019).
42. Y. H. Lin and G. B. Lee, "Optically induced flow cytometry for continuous microparticle counting and sorting," Biosens. Bioelectron. **24**, 572–578 (2008).
43. Y. S. Chen, C. P. K. Lai, C. Chen, and G. B. Lee, "Isolation and recovery of extracellular vesicles using optically-induced dielectrophoresis on an integrated microfluidic platform," Lab Chip **21**, 1475–1483 (2021).
44. C. Witte, J. Reboud, J. M. Cooper, and S. L. Neale, "Channel integrated optoelectronic tweezer chip for microfluidic particle manipulation," J. Micromech. Microeng. **30**, 045004 (2020).
45. T. K. Chiu, W. P. Chou, S. B. Huang, H. M. Wang, Y. C. Lin, C. H. Hsieh, and M. H. Wu, "Application of optically-induced-dielectrophoresis in microfluidic system for purification of circulating tumour cells for gene expression analysis-cancer cell line model," Sci. Rep. **6**, 32851 (2016).
46. W. P. Chou, H. M. Wang, J. H. Chang, T. K. Chiu, C. H. Hsieh, C. J. Liao, and M. H. Wu, "The utilization of optically-induced-dielectrophoresis (ODEP)-based virtual cell filters in a microfluidic system for continuous isolation and purification of circulating tumour cells (CTCs) based on their size characteristics," Sens. Actuators B Chem. **241**, 245–254 (2017).
47. S. Zhang, M. Elsayed, R. Peng, Y. Chen, Y. Zhang, J. Peng, W. Li, M. D. Chamberlain, A. Nikitina, S. Yu, X. Liu, S. L. Neale, and A. R. Wheeler, "Reconfigurable multi-component micromachines driven by optoelectronic tweezers," Nat. Commun. **12**, 5349 (2021).